Compact Parametric Model of Capacitive BAW Resonators

G. Casinovi, A. K. Samarao and F. Ayazi

Joint Conference of the IEEE International Frequency Control Symposium and the European Frequency and Time Forum
pp. 127–130, May 2011

Abstract

This paper presents a new equivalent-circuit model of SiBARs, derived in a mathematically rigorous way from the physics equations governing the behavior of the device. The model is parametric, that is, the model component values can be computed directly from the dimensions of the resonator and the properties of the material. The model also accounts fully, accurately and automatically for aspects of the device behavior that arise from the interaction of multiple physics domain: the shift in the resonance frequency with the polarization voltage (“spring softening”), the effect of the polarization voltage and gap size on the insertion loss, and the reduction in the resonator loaded *Q* as the polarization voltage is increased. In contrast, those effects are not automatically accounted for by other models, such as mass-spring combinations. Finally, the model described is load- and source-independent, and thus it reproduces accurately the behavior of the device itself, regardless of the type and characteristics of the surrounding circuitry.

Copyright Notice

Compact Parametric Model of Capacitive BAW Resonators

Giorgio Casinovi, Ashwin K. Samarao and Farrokh Ayazi
School of Electrical and Computer Engineering
Georgia Institute of Technology
Atlanta, GA 30332, USA

***Abstract*—This paper presents a new equivalent-circuit model of SiBARs, derived in a mathematically rigorous way from the physics equations governing the behavior of the device. The model is parametric, that is, the model component values can be computed directly from the dimensions of the resonator and the properties of the material. The model also accounts fully, accurately and automatically for aspects of the device behavior that arise from the interaction of multiple physics domain: the shift in the resonance frequency with the polarization voltage ("spring softening"), the effect of the polarization voltage and gap size on the insertion loss, and the reduction in the resonator loaded *Q* as the polarization voltage is increased. In contrast, those effects are not automatically accounted for by other models, such as mass-spring combinations. Finally, the model described is load- and source-independent, and thus it reproduces accurately the behavior of the device itself, regardless of the type and characteristics of the surrounding circuitry.**

I. INTRODUCTION

Much research activity in recent years has been directed at the development of bulk acoustic resonators that are compatible with standard integrated circuit technologies. In this respect, capacitive silicon resonators offer a particularly attractive option, since they can be made entirely of materials that are used routinely in IC fabrication processes, resulting in significant advantages in terms of ease of integration and cost savings. For this reason, their use is becoming increasingly common in a wide variety of RF circuits, such as reference oscillators and filters [1].

Disk resonators were among the first examples of micromechanical bulk resonators, but more recently width-extensional-mode resonators based on an alternative, rectangular-bar geometry were demonstrated [2]. In this paper this particular type of capacitive resonators will be referred to as silicon bulk acoustic resonators, or SiBARs. The basic structure of a SiBAR is schematically shown in Fig. 1: the resonating bar element is placed between two electrodes, supported by two thin tethers. A DC polarization voltage applied between the resonator and the electrodes generates an electrostatic field in the capacitive gaps. When an AC voltage is applied to the drive electrode, the electrostatic force applied to the corresponding face of the resonator creates an elastic

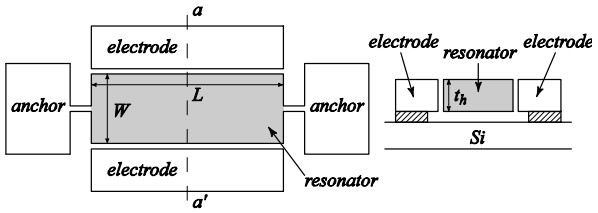

Figure 1. Schematic structure of a SiBAR: top view (left) and cross-sectional view (right)

wave that propagates through the bar. Small changes in the size of the capacitive gap on the other side of the device induce a voltage on the sense electrode, the amplitude of which peaks near the mechanical resonant frequencies of the bar.

While the behavior of bulk resonators is well understood in broad, qualitative terms, sufficiently accurate analytical models of those devices that can be used in place of full-blown finite-element simulation are still lacking. This is a significant drawback in the design of mixed-technology systems that rely on micromechanical resonators. In the simulation of such systems it is common practice to use simple RLC models for the resonators [3][4]. However these models are usually derived using empirical or semi-empirical techniques, often relying on qualitative analogies with similarly behaving systems, such as mass-spring combinations. Consequently, the accuracy of such models cannot be demonstrated or even estimated theoretically: at best, it can only be verified numerically or empirically, and on a case by case basis. In fact, an empirical *RLC* model could not track changes in *Q* and the insertion loss of a silicon bulk acoustic resonator (SiBAR) with the polarization voltage without the introduction of an artificial parasitic resistance [5].

This paper presents an equivalent circuit model of a SiBAR that is derived in a mathematically rigorous way from the governing equations of the device. The model is parametric, in that the model component values can be computed directly from the dimensions of the resonator and the properties of the material. The only exceptions are the resistances in the model, whose values depend on the energy

This work was supported in part by a NSF EAGER grant.

losses in the resonator, which are difficult to model analytically.

The model also accounts fully, accurately and automatically for aspects of the device behavior that arise from the interaction of multiple physics domain: the shift in the resonance frequency with the polarization voltage ("spring softening"), the effect of the polarization voltage and gap size on the insertion loss, and the reduction in the resonator loaded Q as the polarization voltage is increased. In contrast, those effects are not automatically accounted for by other models, such as mass-spring combinations. Finally, the model described in this paper is load- and source-independent, and thus it reproduces accurately the behavior of the device itself, regardless of the type and characteristics of the surrounding circuitry. The model has been validated numerically against finite-element simulations and experimentally against measurements taken on a SiBAR fabricated using the HARPSS process [2].

II. Resonator Model

As in all capacitive MEMS resonators, the operation of a SiBAR is based on the principle of electromechanical transduction. Let W, L and t_h denote respectively the width, length and thickness of the resonator, as shown in Fig. 1. If a DC polarization voltage V_p is applied across the drive and sense capacitive gaps, the resulting electric fields create pressure on the faces of the resonator and a consequent elastic deformation of the structure. If a small-signal voltage v_d is superimposed to the DC voltage at the drive electrode, the change in the electric field in the capacitive gap and the corresponding change in the pressure applied to the resonator face generate an elastic wave that propagates across the width of the resonator.

Therefore a compact SiBAR model can be derived from the equations of elastic wave propagation, under the approximate assumption that the resonant modes of interest are created by the propagation of plane waves in the direction of the width of the resonator. Under this assumption, an analytical solution of the elasticity equations can be obtained. By means of appropriate circuit synthesis methods, this solution is used to derive an equivalent circuit, that is, a circuit the behavior of which is described by the same equations that characterize the operation of the SiBAR.

The resulting equivalent circuit model of the SiBAR is shown in Fig. 2. The values of the circuit elements are given by the following expressions

$$\begin{aligned} C_1 &= C_g/8 & L_1 &= 8/(\omega_0^2 C_g) \\ C_2 &= 2C_g/\pi^2 & L_2 &= \pi^2/(2\omega_0^2 C_g) \\ C_0 &= \varepsilon^2 A^3 c_{33}/WQ_p^2 & R_1R_2 &= (2\pi/\omega_0 C_g)^2 \end{aligned} \tag{1}$$

In the expressions above, Q_p is the value of the DC charge that is present on the drive and sense gap capacitances. Specifically $Q_p = C_g V_p = (\varepsilon A/g)V_p$, where g is the size of the capacitive gap, ε the dielectric permittivity, $A = Lt_h$ and C_g the value of the gap capacitance. Furthermore $\omega_0 = 2\pi f_0$, where f_0 is the mechanical resonance frequency of the resonator, and c_{33} is the stiffness coefficient of the resonator material in the direction of propagation of the elastic waves.

The values of R_1 and R_2 depend on the energy losses in the resonator, that is, on its mechanical Q. Note that (1) imposes a constraint on the product R_1R_2. Consequently the value of only one of those resistors can be chosen independently. For example, the measured ratio between the input voltage and the short-circuit output current of the SiBAR at resonance can be used for this purpose. An approximate but sufficiently accurate expression for this ratio can be obtained by observing that near the resonant frequency the current through the series $R_2L_2C_2$ circuit will dominate the current through the parallel $R_1L_1C_1$ circuit: it is therefore reasonable to assume that $i_3 \cong i_4$. After some algebraic manipulations, the following expression is obtained

$$i_s = \frac{j\omega C_g/L_2C_0}{-\omega^2 + j\omega(R_2/L_2) + (1-2C_2/C_0)/(L_2C_2)} v_d \tag{2}$$

The expression above shows that the electrical resonant frequency ω_1 — i.e. the frequency at which i_s achieves its maximum value — is lower than the mechanical resonant frequency ω_0 and is given by

$$\omega_1 = \omega_0\sqrt{1-2C_2/C_0} \tag{3}$$

In particular, since the value of C_0 depends on the DC bias voltage V_p, so does the value of ω_1. This is a well-known effect, which has been consistently observed in experimental setups [3][5]. Setting $\omega = \omega_1$ in (2) yields the desired

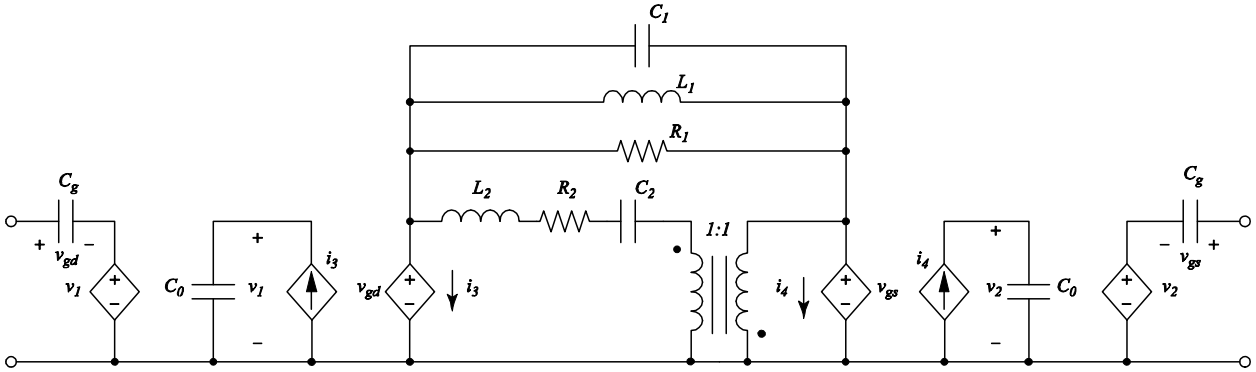

Figure 2. SibAR equivalent circuit model

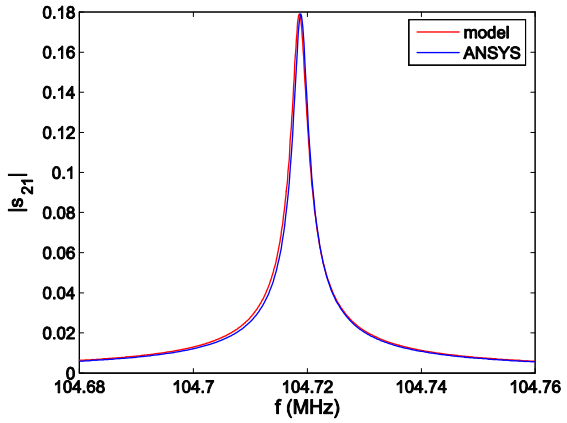

Figure 3. SiBAR s_{21} parameter extracted from simulations

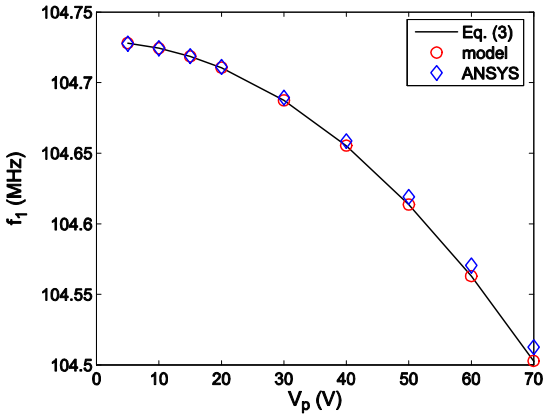

Figure 4. SiBAR electrical resonance frequency vs. polarization voltage

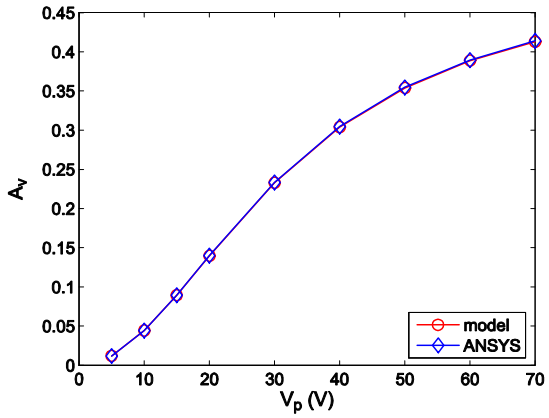

Figure 5. SiBAR voltage gain at resonance vs. polarization voltage

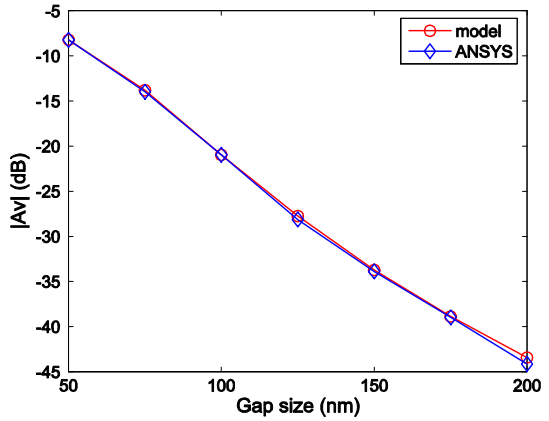

Figure 6. SiBAR voltage gain at resonance vs. capacitive gap size

relationship between the value of R_2 and the v_d/i_s ratio at resonance, namely

$$R_2 = \frac{C_g}{C_0}\left(\frac{v_d}{i_s}\right)_{\omega=\omega_1} \tag{4}$$

Note that once the value of R_2 has been computed for a particular geometry, it can be extrapolated to other geometries if the rate of energy loss in the resonator does not change.

Further improvements to the model can be made by solving the elasticity equations more accurately, taking the finite thickness of the resonator into account [6]. Because of space limitations the calculations are omitted here, but the end result is a modified expression for C_0, while the rest of the equivalent circuit model remains unchanged.

III. Numerical Simulations

The equivalent circuit model described in the previous section was compared to finite-element simulations of a SiBAR performed in ANSYS. A detailed description of the ANSYS model is given in [6]. The device used in the comparisons was a resonator of dimensions L = 400 µm, W = 40 µm, t_h = 20 µm, with a DC bias voltage V_p = 15 V. Fig. 3 compares the s_{21} parameter obtained from an ANSYS simulation of the device with 50 Ω source and load resistances with the s_{21} parameter of the model under the same conditions.

A second set of simulations was then performed on the same device with various DC polarization voltages, ranging from 5 V to 70 V, while keeping the values of the source and load resistances fixed at 50 Ω. Fig. 4 shows the electrical resonant frequency $f_1 = \omega_1/2\pi$ of the device at each value of V_p, obtained both from ANSYS and model simulations. The same figure shows also the graph of the relationship between f_1 and V_p given by (3). It can be seen that the simulation results track very closely the relationship in (3), which in turn matches actual measurements taken on SiBARs, as will be shown in Sec. IV. Fig. 5 shows the value of the voltage gain $A_v = v_{out}/v_{in}$ at resonance as a function of V_p, obtained both from ANSYS and model simulations.

A final set of simulations was performed to evaluate the effect of the size of the capacitive gaps on the voltage gain of the device. It should be noted that for these simulations the values of R_1 and R_2 were changed assuming an inversely proportional relationship to C_g. This assumption stems from the fact that R_1 and R_2 are determined by the mechanical Q of the resonator, which is independent of the gap size. Based on the expressions in (1), keeping the Q of resonant circuits

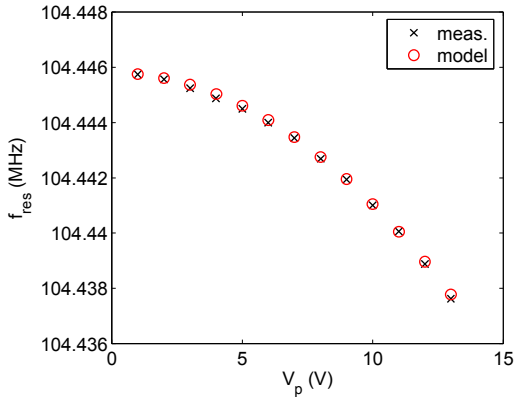

Figure 7. SiBAR resonance frequency predicted by the model compared to measured values

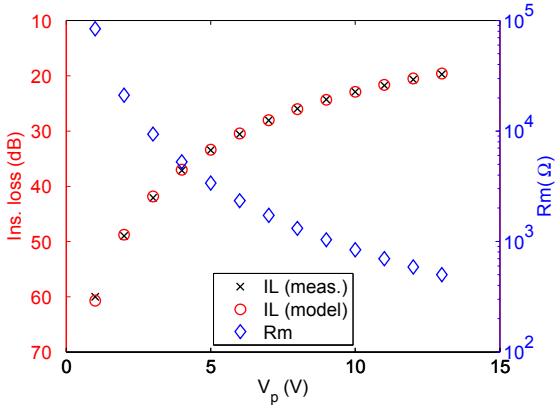

Figure 8. Left axis: SiBAR insertion loss predicted by the model compared to measured values. Right axis: SiBAR motional resistance

$R_1L_1C_1$ and $R_2L_2C_2$ constant with the gap size requires the resistance values to be inversely proportional to C_g. The results of this last set of simulations obtained from the model and from ANSYS are shown in Fig. 6. It can be seen that in all cases the graphs in the figures show excellent agreement between the two sets of data, a result that clearly supports the validity of the model.

IV. Experimental Model Validation

In addition to finite-element simulations, the SiBAR model was validated experimentally against measurements taken on a device fabricated using the HARPSS process [2]. The nominal dimensions of the device were L = 400 µm, W = 40 µm, t_h = 20 µm. The extracted values of the width and gap size were W = 40.028 µm and g = 99 nm, respectively. Fig. 7 compares the measured resonance frequency of the device with that predicted by the model, as a function of the polarization voltage V_p. Fig. 8 shows a similar comparison for the insertion loss of the device, also as a function of V_p. For reference purposes, the corresponding values of the motional resistance R_m are also plotted. Finally, the values of the quality factor Q of the device, both measured and predicted by the model, are plotted versus V_p in Fig. 9. Although the agreement is not as good as in the two previous figures, it can be seen that the

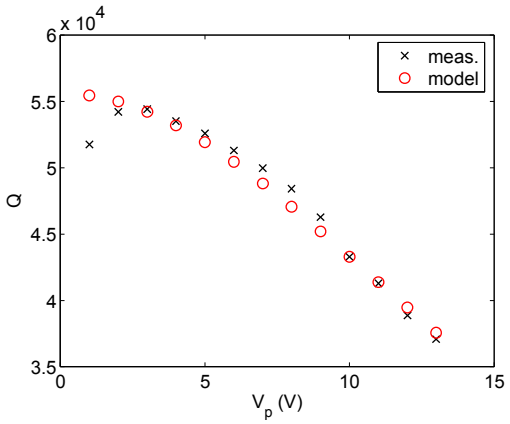

Figure 9. SiBAR quality factor Q predicted by the model compared to measured values

model tracks with good accuracy the drop in Q with the increase in V_p without introducing an artificial additional resistance, which is instead needed in simpler, empirically derived resonator models [5].

V. Conclusion

This paper has introduced a parametric equivalent circuit model for SiBARs that is derived directly from the equations governing the electromechanical behavior of the device. Consequently the values of most of the components in the model can be computed analytically, based on the dimensions of the resonator and the properties of the material. The only model parameters that cannot be determined in this way are the resistance values, which are tied to energy losses in the device. Simulation results show that the performance parameters extracted from the model are in excellent agreement with those obtained both from finite-element analysis of the device and from actual measurements. Thus the model can be profitably used in the design of complex mixed-technology circuits that include SiBARs among their components, such as VHF oscillators.

References

[1] C. T.-C. Nguyen, "MEMS technology for timing and frequency control," *IEEE Trans. Ultrason., Ferroelect., Freq. Contr.*, vol. 54, no. 2, pp. 251–270, Feb. 2007.

[2] S. Pourkamali, G. K. Ho, and F. Ayazi, "Low-impedance VHF and UHF capacitive silicon bulk acoustic wave resonators — Part I: Concept and fabrication," *IEEE Trans. Electron Devices*, vol. 54, no. 8, pp. 2017–2023, Aug. 2007.

[3] J. Wang, Z. Ren, and C. T.-C. Nguyen, "1.156-GHz self-aligned vibrating micromechanical disk resonator," *IEEE Trans. Ultrason., Ferroelect., Freq. Contr.*, vol. 51, no. 12, pp. 1607–1628, Dec. 2004.

[4] J. R. Clark, W.-T. Hsu, M. A. Abdelmoneum, and C. T.-C. Nguyen, "High-*Q* UHF micromechanical radial-contour mode disk resonators," *J. Microelectromech. Syst.*, vol. 14, no. 6, pp. 1298–1310, Dec. 2005.

[5] S. Pourkamali, G. K. Ho, and F. Ayazi, "Low-impedance VHF and UHF capacitive silicon bulk acoustic wave resonators — Part II: Measurement and characterization," *IEEE Trans. Electron Devices*, vol. 54, no. 8, pp. 2024–2030, Aug. 2007.

[6] G. Casinovi, X. Gao, and F. Ayazi, "Lamb waves and resonant modes in rectangular-bar silicon resonators," *J. Microelectromech. Syst.*, vol. 19, no. 4, pp. 827–839, Aug. 2010.